Determining the key drivers of magnetospheric Pc5 wave power

L. E. Simms,[1] V. A. Pilipenko,[2] and M. J. Engebretson[1]

Received 30 October 2009; revised 4 May 2010; accepted 11 May 2010; published 22 October 2010.

[1] Long-period ground ULF waves may be controlled by the mean values of solar wind and interplanetary magnetic field (IMF) parameters (velocity, density, and North-South IMF component *Bz*). We investigated the influence of these parameters on ground ULF power in the Pc5 range (2–7 mHz) during periods of quiet and during coronal mass ejection (CME) and corotating interaction region (CIR) storms from 1991 to 2004. With multiple regression and path analysis, we studied the influence of these hourly parameters as a set rather than individually. This allowed us to determine which factors were most influential and which were only correlated with influential factors. By using multiple regression, we have explained more variation in Pc5 power than has been achieved in previous studies. In both storm types (CME and CIR) and during all storm phases (initial, main phase, recovery, and a 48 h period after recovery) as well as during quiet periods, solar wind velocity and IMF *Bz* influenced ground Pc5 power directly. These two variables also acted on the ULF Pc5 indirectly through the intermediate parameters of *Dst*, and the variations in number density and IMF, although at a weaker level. Ground Pc5 power was greater during CME storms during the main phase and recovery but larger during CIR storms in the period after recovery. In addition, the effect of certain independent variables differed depending on storm type. A model such as this offers the possibility of nowcasting Pc5 power by inserting current levels of solar wind and IMF variables as predictors into the regression equation.

Citation: Simms, L. E., V. A. Pilipenko, and M. J. Engebretson (2010), Determining the key drivers of magnetospheric Pc5 wave power, *J. Geophys. Res.*, *115*, A10241, doi:10.1029/2009JA015025.

1. Introduction

[2] The interactions between the Earth's magnetosphere and the solar wind appear to drive much of the activity seen in the magnetosphere. The periodic response in the Pc5 range to solar wind driving may be due to the occurrence of natural MHD resonators or waveguides in the magnetosphere. For this reason, the generation of magnetospheric Pc5 waves by the solar wind has often been studied using the assumption of laminar plasma flow, where the magnetosphere resonates at frequencies determined by its own internal properties rather than as a result of external pulsations. Indeed, the ultralow frequency (ULF) wave activity in the Pc5 range observed at ground magnetometers is enhanced by increased solar wind velocity [*Greenstadt et al.*, 1979; *Engebretson et al.*, 1998; *Vennerstrom*, 1999; *Mathie and Mann*, 2001; *Baker et al.*, 2003; *Posch et al.*, 2003; *Pahud et al.*, 2009]. However, pulsations within the Earth's magnetosphere may be the result of forced oscillations induced by solar wind density/pressure variations [*Kepko et al.*, 2002; *Kepko and Spence*, 2003; *Posch et al.*, 2003; *Eriksson et al.*, 2006; *Takahashi and Ukhorskiy*, 2007, 2008; *Kessel et al.*, 2004; *Villante et al.*, 2007; *Kessel*, 2008] or from turbulence in the solar wind magnetic field [*Borovsky and Funsten*, 2003; *Villante et al.*, 2007]. The power spectra of the upstream solar wind fluctuations and magnetospheric ULF magnetic variations in the Pc5 band were found to be similar, suggesting that fluctuations of the solar wind are triggering the ULF waves in the magnetosphere, although the nature of these quasi-periodic solar wind fluctuations and the mechanism of their transmission through the magnetosheath are still practically unknown. Besides compressional fluctuations, the ULF ground response to the noncompressive fluctuations of the IMF has also been noted [*Villante et al.*, 2006].

[3] Pc5 wave activity has been suggested as an intermediary between the solar wind flow and relativistic electron dynamics, causing their radial transport and acceleration [*O'Brien et al.*, 2001], and a good correlation is seen between increases in these electrons and Pc5 wave power in the days just preceding this rise [*Elkington et al.*, 2003; *Mann et al.*, 2004; *Mathie and Mann*, 2000]. Thus, the construction of any realistic model of relativistic electron dynamics would demand a knowledge of statistical relationships characterizing the Pc5 response of the magnetosphere to solar wind/IMF driving.

[4] However, most of the previous statistical studies examine the role of various solar wind processes in gener-

[1]Department of Physics, Augsburg College, Minneapolis, Minnesota, USA.
[2]Institute of the Physics of the Earth, Moscow, Russia.

0148-0227/10/2009JA015025

ating magnetosphere pulsations by considering one parameter at a time, even though all the solar wind parameters are mutually correlated to varying degrees. Relationships between the various solar wind parameters and magnetospheric pulsations are complex and should be studied as a whole, rather than in isolation, to more completely understand the associations. To this end, we have chosen in this paper to study the association of Pc5 wave power at ground magnetometers with a variety of solar wind/IMF parameters, examining the data with multiple regression analysis. This method of analysis allows comparisons of associations of parameters and their influence on the dependent parameter (ground Pc5 wave power) to be studied as a whole rather than individually. In addition, we were able to use the method of path analysis to study a presumed structure of interactions among the variables.

[5] It is possible that Pc5 pulsations respond differently to variations in the solar wind and IMF depending on whether a storm is triggered by a coronal mass ejection (CME) or a corotating interaction region (CIR). Therefore, we first analyze CME and CIR storms separately. As they result from different solar processes, CME storms from the ejection of material from the Sun and CIR storms from large-scale structures in the heliosphere involving the interaction of fast and slow solar winds [*Tsurutani et al.*, 1995], it is not surprising that the response of the Earth's magnetosphere differs for the two. CME storms, on average, produce a greater drop in *Dst* [*Gonzalez et al.*, 1999; *Alves et al.*, 2006; *Denton et al.*, 2006]. Because CIR storms show a greater efficiency at depositing energy into the magnetosphere, their energy input may overall be higher [*Turner et al.*, 2009]. We also perform a second set of multiple regressions that include all CME and CIR storms together that explore the differences between these storm types.

2. Database

[6] We identified 480 storms with usable data occurring between 1991 and 2004. Of these, 377 could be classified as CME (169 storms) or CIR (208 storms), although in some instances storms might not have usable data for the entire storm period. Quiet periods were obtained by removing all storm hours from the data set, as well as the 24 h period before storm onset and 48 h after the end of recovery. We removed all hours from the data set for which there was not complete coverage of the variables.

[7] As a measure of magnetospheric wave power in the Pc5 range (2–7 mHz), we use the hourly ground ULF wave index, T_{GR} [*Kozyreva et al.*, 2007]. The ULF wave index has been successfully used in statistical studies of various space physics problems [*Romanova and Pilipenko*, 2009; *Pilipenko et al.*, 2008]. This index is calculated from 1 min ground magnetometer stations in the Northern Hemisphere during the 14 years from 1991 to 2004. To quantify the short-term IMF and solar wind variability in the Pc5 range, we use the interplanetary ULF wave power indices, T_{IMF} and T_N, estimated using 1 min data from one of the available interplanetary satellites.

[8] The data were split into periods corresponding to the initial phase of a storm, main phase, recovery, a 48 h period after recovery, and quiet. Storms were identified when *Dst* dropped below −30 nT and IMF *Bz* below −5 nT. The main phase was defined as the period from the first drop in *Dst* until the minimum *Dst* was reached. The initial phase may last from 1 to 6 h before the main phase onset; however in our statistical analyses, we used only the 1 h before the *Dst* drop so as to be sure all our data in this category were, in fact, from the initial period of the onset of the storm. We identified recovery as the period from minimum *Dst* until *Dst* reached −30 nT, and after recovery was identified as the 48 h after *Dst* returned to −30 nT. The data set was further subsetted into CME versus CIR storms. We used the list of CME events given by I. Richardson and H. Cane (www.ssg.sr.unh.edu/mag/ace/ACElists/ICMEtable.html) to classify storms from 1996 onward. Storms were labeled as CME if a CME event was occurring. If the list had no CME events during a given storm period, then storms were labeled as CIR. Before 1996, we used the classification of *Yermolaev et al.* [2009] that classifies storms as CIR, CME, or magnetic cloud (MC). We identified the MC category as CME as well. Before 1996, many storms were unclassified, and these were left out of the analysis.

[9] In addition to analyzing the data by storm type, we also combined CME and CIR data to perform a full regression analysis for each storm time including storm type as an additional independent indicator variable (with a value of 1 for CME storms and −1 for CIR storms). We included the interaction terms for storm type with each of the other independent parameters. This gave information on whether magnetospheric Pc5 pulsations were statistically different between CME and CIR storms, as well as whether the effect of the other parameters differed by storm type.

3. Statistical Approach and Tools

[10] Our main goal was to study the influence of a set of solar wind and IMF parameters on Pc5 power. To accomplish this, we used multiple regression and path analysis. This allowed us to compare the influence of factors while all other factors were accounted for.

[11] We tested the predictive power of solar wind speed bulk speed (*V*), plasma density (*N*), IMF North-South component *Bz* (in the GSM coordinate system), *Dst* (as a measure of the ring current intensity), and the fluctuations of number density and IMF *B* in the Pc5 range characterized by the indices T_N and T_{IMF}. (Spectral power of IMF fluctuations in the Pc5 band is calculated as the sum of powers of its components, $T_{IMF} = T_{Bx} + T_{By} + T_{Bz}$. In this study we do not separate compressional and noncompressional fluctuations of IMF.) We hypothesized that velocity, plasma density, and *IMF Bz* would drive the levels of number density variation, IMF variation, and *Dst*. The six of these variables would then, in concert, act on the ground Pc5 wave power (T_{GR}). We represent this structure with a path analysis, allowing a visual representation of a series of multiple regressions. The goal of path analysis is to give estimates of the magnitude of correlational links between variables. The dependent variable is predicted by all the independent variables, but several of the independents may also be predicted by other independents. Thus, some independent variables may have both direct effects on the ultimate dependent variable and indirect effects by their influence on other independent variables. Statistical analyses were performed using SPSS (SPSS Inc., 2005, Chicago, IL, USA).

Table 1. Correlations of Solar Wind Density *N*, Velocity *V*, IMF *Bz* Pressure *P*, and Electric Field *Ey*[a]

Correlated Pair	Initial	Main Phase	Recovery	After Recovery
		CME Storms		
P-N	0.815*	0.700*	0.806*	0.850*
P-V	0.293*	0.405*	0.179*	0.140*
N-V	−0.235*	−0.160*	−0.283*	−0.265*
Ey-Bz	−0.977*	−0.958*	−0.966*	−0.982*
Ey-V	−0.372*	0.067*	−0.219*	−0.008
Bz-V	0.326*	0.099*	0.182*	−0.041*
		CIR Storms		
P-N	0.836*	0.819*	0.784*	0.744*
P-V	0.129	−0.028	0.078*	0.154*
N-V	−0.334*	−0.459*	−0.447*	−0.443*
Ey-Bz	−0.974*	−0.975*	−0.977*	−0.979*
Ey-V	−0.454*	−0.124*	−0.176*	−0.035*
Bz-V	0.368*	0.220*	0.221*	0.035*

[a]Values with asterisk are statistically significant at confidence level $P < 0.05$.

[12] Although the solar wind dynamic pressure $P = NV^2$ and electric field $Ey = -VB_z$ have been used with success in statistical studies of solar-terrestrial relationships, we did not use them in our regressions because they are mathematically derived from the measured parameters and are therefore highly correlated with them. In particular, *P* is highly correlated with *N* (Table 1), with correlation coefficients ranging from 0.70 to 0.85. Similarly, the correlation of *Ey* with *Bz* ranges from −0.96 to −0.98. These high correlations between independent variables can make conclusions about the influence of individual independent variables invalid [*Neter et al.*, 1985]. Also, as our intent was to present these analyses as path analyses, we were also interested in keeping the models manageable to facilitate interpretation. Given that we could only reasonably use either the derived variables (*P* and *Ey*) or the measured variables (*N*, *V*, and B_z), we chose to use the measured parameters. We believe this gives more insight into the actual processes occurring. However, to determine whether this resulted in a more predictive model, we first ran regression models using each of these sets of parameters (Table 2). For each regression model, we report the coefficient of determination (R^2). In all data categories (initial, main phase, recovery, the 48 h after recovery, and quiet), the models using the measured parameters (*N*, *V*, and *Bz*) have a higher predictive value than those using the derived parameters (*P* and *Ey*). It is true that the first model, with three independent parameters, may have a higher R^2 only because a greater number of parameters increase the number of degrees of freedom in the model. In situations where variables are added to an existing model, the adjusted R^2 statistic corrects for the increase in the degrees of freedom [*Neter et al.*, 1985]. This is not strictly applicable to the situation we present here where two different models are being compared but may provide a helpful estimate of the difference made by adding another variable to the model. In four of the time periods (main phase, recovery, after recovery, and quiet), the R^2 and adjusted R^2 were identical for each model. In the initial phase, the adjusted R^2 was lower for both models but was still greater for the model using *N*, *V*, and B_z than that using the derived parameters. As the models using the measured parameters always show a higher R^2 (even when adjusted for the differing number of parameters), it is preferable to use measured parameters instead of derived variables in modeling Pc5 activity.

[13] Much work has shown that Pc5 intensity responds differently to northward and southward IMF *Bz* (see references above); however, we decided not to split our data into categories on the basis of this dichotomy. Observations show that the direction of the IMF changes rapidly, often hourly. If we were to break our analyses into northward and southward categories, we would be unnaturally separating observations that occur together in time. As we were interested in the time progression of these processes, we chose to keep observations together based on their occurrence in time.

[14] As a comparison to other studies, we first report the simple correlations between T_{GR} and the individual predictor variables *X*. In addition, we explored whether the relationship between T_{GR} and each predictor was best fit by a linear, exponential, or power model. The three models are as follows:

$$\begin{aligned} \text{Linear}: &\quad T_{GR} = b_0 + b_1 X \\ \text{Exponential}: &\quad T_{GR} = 10^{b_0 + b_1 X} \\ \text{Power}: &\quad T_{GR} = b_0 X^{b_1} \end{aligned} \tag{1}$$

Although a few variables occasionally showed a better fit using a linear model in the simple correlations, the multiple regressions were performed with $\log_{10} T_{GR}$ as this consistently fit more of the variables. As several of the most correlated parameters in the single correlations (*V*, T_{IMF}, T_N, *Bz*) showed a power or exponential relationship with T_{GR}, the best fit in the multiple regressions for these more correlated parameters can only be obtained if the dependent variable (T_{GR}) is log-transformed. This made it impossible, in a multiple regression, to follow the best fit for the few variables that sometimes followed a linear relationship while still fitting the rest of the variables to an exponential or power model. The log transformation produces a model in which the dependent variable is affected multiplicatively by the independent variables rather than additively.

[15] Simple correlations (reporting the correlation coefficient, *r*) are comparable to simple linear regression, in that the correlation coefficient is the same as the coefficient obtained from the simple regression model with only one predictor variable. However, to compare regression models in which there are more than one independent variable, a different statistic is used, the coefficient of determination, R^2. The R^2 value gives an estimate of the proportion of

Table 2. Coefficient of Determination for Multiple Regression Models Predicting T_{GR} Using Density, Velocity, and IMF *Bz*, and Pressure and Electric Field for All Storms Together

Independent Variables	*N*, *V*, *Bz*	*P*, *Ey*
Initial phase	0.269	0.065
Main phase	0.330	0.181
Recovery	0.337	0.197
After recovery	0.391	0.184
Quiet	0.386	0.173

Table 3. Durbin-Watson Statistics for the Multiple Regression Models With and Without Lag Term Where T_{GR} is Lagged by 1 Hour[a]

Storm Type	n	No Added Lag Term	Added Lag Term
		Main Phase	
CME	1796	1.210	2.069
CIR	2930	1.144	2.042
		Recovery	
CME	4230	1.036	2.062
CIR	3210	1.247	2.043
		After Recovery	
CME	5139	1.118	2.027
CIR	8060	1.222	2.015
		Quiet	
	51,092	1.030	2.038

[a]Here n is the number of hourly observations.

variability in the dependent variable that is accounted for by the regression model [*Neter et al.*, 1985]. It estimates how well the model predicts the level of the dependent variable. The correlation coefficients r can be easily converted to R^2 by squaring them. To allow easy comparison to previously published work, we have presented not only the R^2 determined by the multiple regressions but also the simple correlations r.

[16] For ease of comparing between multiple regression models and the path diagrams (see below), we chose to pick one approach to modeling each of the independent variables in all the multiple regressions. For example, rather than attempting to compare T_N in a power relation to T_{GR} in one multiple regression, followed by T_N in an exponential model in the next, we used only the power relationship for T_N for all analyses. The choice was determined by which model fit a particular variable best in the simple correlations for the majority of cases. A power model was chosen for T_N and T_{IMF}, whereas an exponential model was chosen for V, N, Bz, and Dst. In practice, this meant that T_{GR}, T_{IMF}, and T_N were log-transformed, whereas V, N, Bz, and Dst were not.

[17] Except for the initial phase data, which consists of a single observation in the hour before the main phase of each storm, all other categories of data were made up of time series, with observations spaced only 1 h apart. This type of data often shows serial autocorrelation, with a variable at one time step being highly dependent on its own value in previous time steps. This can seriously impact interpretations from regression models if the autocorrelation is not corrected. The Durbin-Watson statistic tests for serial autocorrelation, detecting the presence of autocorrelation in the residuals from a regression analysis [*Neter et al.*, 1985]. If there is no autocorrelation, a value of 2 is obtained. If the Durbin-Watson statistic is substantially less than 2, this is evidence of positive serial autocorrelation (where an observation is positively correlated with its own value in previous time steps). In all data categories, the Durbin-Watson statistic calculated from the residuals of the multiple regression analysis showed there was positive autocorrelation (next to last column in Table 3). When the same regression was run with the 1 h lag of T_{GR} added as an independent variable (to correct for the autocorrelation), this problem disappeared (last column in Table 3). These regressions with the added lag term were used in the subsequent analyses. During the initial phase, when only 1 h is used in the analysis, we also added the 1 h lag term although it was not necessary to correct for serial autocorrelation. In this case, we did this to allow comparisons between analyses of the initial period with the other periods.

[18] Using the regression models, we performed a path analysis for each data category. The goal of path analysis is to give estimates of the magnitude of correlational links between variables. The dependent variable may be predicted by all the independent variables, but several of the independents may also be predicted by other independents. Thus, some independent variables may have both direct effects on T_{GR}, as well as indirect effects by their influence on other independent variables.

[19] The results of path analysis can be shown with a path diagram [*Loehlin*, 1991]. Each path in the diagram is given a weight representing the influence of one variable on another. These weights are the standardized regression coefficients, determined from a series of multiple regression analyses. In the first analysis, T_{GR} is the dependent variable and weights are assigned to those paths, called the direct paths, leading directly from each independent variable (T_N, T_{IMF}, Dst, N, V, and Bz) to T_{GR}. However, as T_N, T_{IMF}, and Dst are theorized to depend on N, V, and Bz, three more regressions are then performed with T_N, T_{IMF}, and Dst as the dependent variables and N, V, and Bz as the independents. These regressions give the weights for paths from N, V, and Bz to these intermediate variables. The final result is a diagram (with coefficient weights for each pathway) that shows the effects of all the parameters on T_{GR}, as well as paths that show the effects of N, V, and Bz on T_N, T_{IMF}, and Dst. These latter paths are called the indirect paths. The series of regressions performed to determine the coefficients for the path diagram would be:

$$\begin{aligned}
\log_{10} T_{GR} &= b_{11} \log_{10} T_N + b_{12} \log_{10} T_{IMF} + b_{13} Dst + b_{14} N \\
&\quad + b_{15} V + b_{16} Bz + b_{17} Lag T_{GR} \\
\log_{10} T_N &= b_{21} N + b_{22} V + b_{23} Bz \\
\log_{10} T_{IMF} &= b_{31} N + b_{32} V + b_{33} Bz \\
Dst &= b_{41} N + b_{42} V + b_{43} Bz
\end{aligned} \tag{2}$$

with each b_{ij} being the standardized regression coefficient to be used in the path diagram.

[20] The overall effects of V, N, and Bz on T_{GR} may be more than just their direct effect as they also influence the intermediate variables T_N, T_{IMF}, and Dst. The overall effect of V, N, and Bz can be calculated by adding the coefficient of the direct path to the multiplied product of the indirect paths. For example, the total effect of each of V, N, and Bz (represented as X_i in equation 3) on Y (T_{GR}) would be calculated by

$$\begin{aligned}
&(\text{coefficient of } X_i \text{ on } Y) + \sum_j \big(\text{coefficient of } X_i \text{ on } X_j\big) \\
&\quad \cdot \big(\text{coefficient of } X_j \text{ on } Y\big).
\end{aligned} \tag{3}$$

[21] Path diagrams are a convenient tool for displaying our hypotheses about the relationships of variables. They do not, in themselves, prove the causal relationships shown but

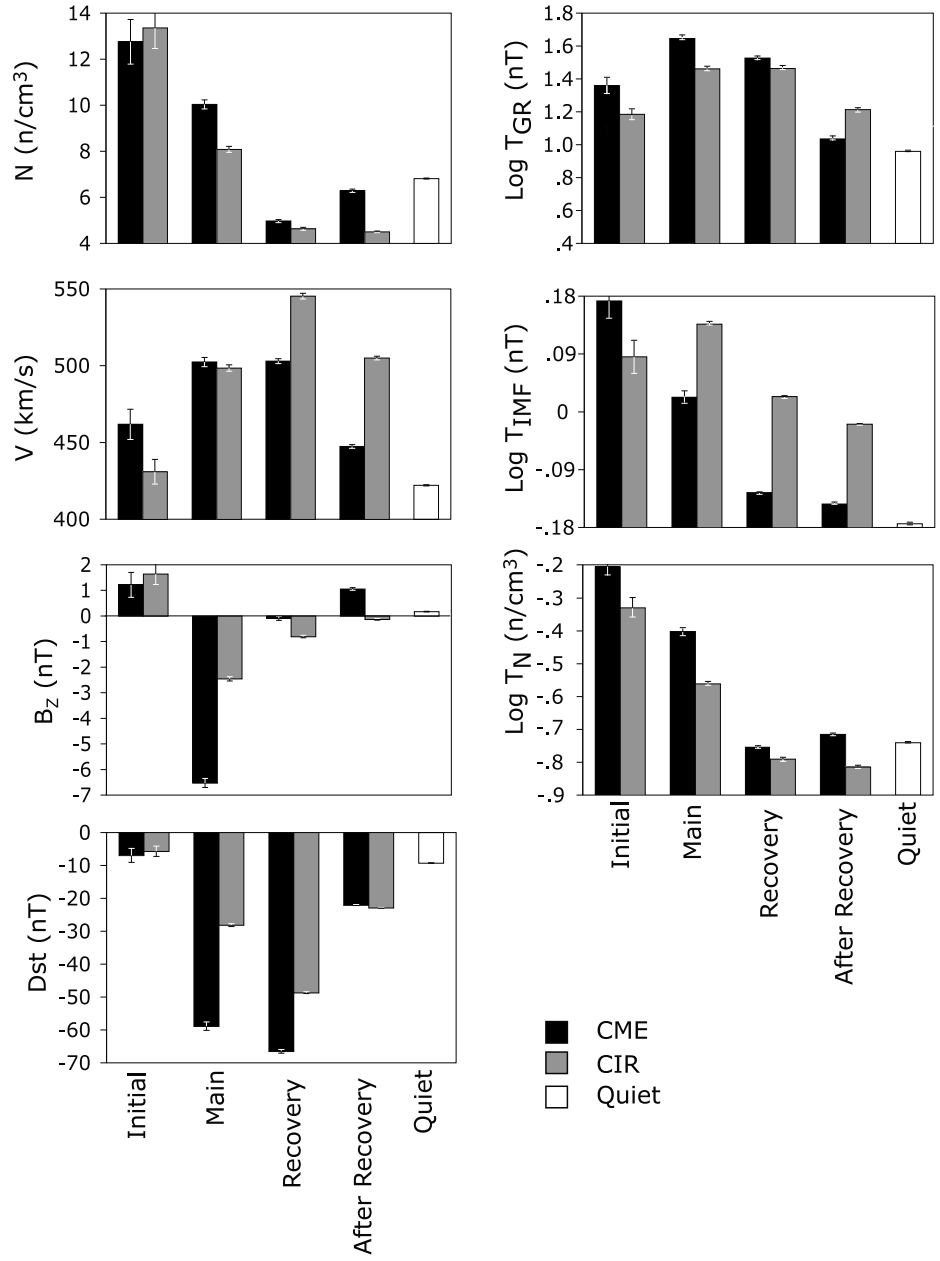

Figure 1. Mean and standard error of the parameters broken down by phase of the storm (initial, main, recovery, 48 h after recovery) and type of storm (CME or CIR).

only demonstrate how the correlations among the variables would behave in this particular data set if our assumptions of causality are true. For convenience, as we describe our results, we often refer to the correlations as implying a causal relationship.

4. Statistical Results

[22] Figure 1 shows the means and standard errors of each parameter averaged over each phase of the storm. During the main phase of CME and CIR storms, the solar wind velocities are statistically nearly the same, but for CME storms, the density increase and IMF *Bz* negative excursion are larger than for other storms. *V* grew over the average course of the storms and was highest in recovery, with CIR storms showing the highest average. The *Dst* response shows a predictable intensification during the main phase, largest for CME storms. Counterintuitively, the average *Dst* is lower in recovery than during the main phase, but this is because the *Dst* is at a higher level at the start of the main phase than it ever returns to before the end of recovery.

[23] The solar wind and IMF fluctuation levels, T_N and T_{IMF}, are larger for CME storms during the initial phase. During the main phase, the CME storms are also accompanied by more intense fluctuations of *N* than CIR storms, whereas IMF fluctuations are greater in CIR storms.

[24] The ULF ground response varies depending on the type of storm and the phase of the storm. The T_{GR} index was

lowest during quiet periods. During storms, the index tended to be lower during the initial phase and in the 48 h after recovery. During the main phase, T_{GR} was higher during CME storms as opposed to CIR storms. However, in recovery the difference between CME and CIR storms lessens. T_{GR} in the 48 h after recovery is greater in CIR storms.

[25] However, the averages given in Figure 1 do not show the progression of these parameters over the course of the storms. This is better seen in an average epoch time plot (Figure 2). In Figure 2, the linear values of *Dst*, *N*, *V*, and *Bz* and the $\log_{10}$ of T_{GR}, T_{IMF}, and T_N are plotted. Using the first drop in *Dst* as the marker between the initial and main phase, and the lowest value of *Dst* as the marker between main phase and recovery, hourly data for CME and CIR storms were averaged and plotted. Figure 2 plots are divided into a pre-storm period (24 h before the start of the main phase), main phase (from the *Dst* drop until the lowest *Dst*), and then 6 h before recovery (i.e., 6 h before the lowest *Dst*), and the 48 h period following the start of recovery.

[26] In the epoch average time plots, CME storms (solid line) tend to be stronger storms, with lower *Dst* and stronger IMF *Bz* in the main phase. For the most part, *N* is somewhat higher in CME storms during all phases, whereas *V* becomes higher in CIR storms during the recovery phase and after it.

[27] The IMF variability, as characterized by T_{IMF}, is higher during CIR storms at all times except for the pre-storm period. On the other hand, the plasma variability, T_N, is generally higher in the CME storms. It is interesting that the solar wind and IMF variability start to grow statistically at least 6 h before the storm onset. This may indicate "precursory" behavior in the solar wind and IMF properties before the storm onset.

[28] For both types of storms, the T_{GR} wave index rises sharply in the hours before the *Dst* drop and remains elevated during the first hours of the main phase, but T_{GR} begins its rise earlier and reaches a higher level in the CME storms throughout the pre-storm period and main phase. In fact, the T_{GR} is slightly higher during the whole 24 h period before the onset of the storm in CME storms. During recovery and the time period after recovery, T_{GR} is similar between CME and CIR storms, although it drops off faster in CME storms some hours into this period as has also been noted by *Borovsky and Denton* [2006]. Thus, CIR storms, despite their lower geoeffectiveness as measured by *Dst*, are more effective in generating Pc5 wave activity in the later hours of the recovery phase and the period after recovery, probably because of a higher solar wind velocity. The current version of the ULF index, based on band-integrated spectral power, does not discriminate between the narrowband monochromatic Pc5 waves and irregular wideband variations. Most probably, the rise of the ULF index during the main phase is due to irregular magnetic variations (sometimes called Pi3), whereas an elevated level of the ULF index at the recovery phase is caused by the occurrence of quasi-monochromatic Pc5 pulsations.

[29] Of the variables thought to be drivers of the T_{GR} waves, many have time plots similar to that of the Pc5 wave power at certain points, but none of the time plots show an exact match to that of the T_{GR} time plot. This suggests that more than one factor is responsible for driving the Pc5 wave power and the relative contribution of these factors vary during the storm evolution.

4.1. Nature of the Relationship Between ULF Wave Power and the Independent Interplanetary Parameters

[30] We analyze the correspondence of various forms of dependencies: linear, power, and exponential, between the Pc5 wave power and independent parameters of the solar wind and IMF (Figure 3). The power model is modeled in linear regression by log transforming both dependent and independent variables. As both *Dst* and *Bz* contain both positive and negative values, only the linear and exponential models were tested with them.

[31] A power model best describes the relationships between T_{GR} and T_{IMF} and T_N in the majority of data categories. In a few categories, the exponential model fit the data slightly better, and even when the power model had a higher correlation, the exponential model was not far behind. A power model best described the correlation of T_{IMF} with T_{GR} in 6 out of the 9 categories (and tied with the exponential in one category). The power relationships gave the highest correlation with T_N in 7 out of 9 categories. The somewhat greater number of categories where the power model was better than the exponential convinced us to use the power model for T_{IMF} and T_N in the multiple regressions. The power relationship of T_{IMF} and T_N with T_{GR} is described by $T_{GR} \propto T_{IMF}^{\alpha_{IMF}}$, where $\alpha_{IMF} = 0.52$ during storms and $\alpha_{IMF} = 0.51$ during quiet periods, and $T_{GR} \propto T_N^{\alpha_N}$, where $\alpha_N = 0.23$ in storms and $\alpha_N = 0.09$ in quiet.

[32] For *N* and *V*, the power and exponential models were, for the most part, fairly equal in their correlations. In some categories, the linear model was by far the worst model, making this an inappropriate choice for the multiple regression analysis, but the choice between power and exponential was not as clear. We chose to use the exponential model in the multiple regressions but report the power relationships here to aid comparison to other studies: $T_{GR} \propto V^{\alpha_v}$, where $\alpha_v = 2.1$ during storms, $\alpha_v = 2.5$ in quiet, and $T_{GR} \propto N^{\alpha_N}$, where $\alpha_N = 0.13$ in storms, and $\alpha_N = -0.08$ in quiet.

[33] The simple correlations of Figure 3 also indicate that a number of the possible explanatory variables might be useful in predicting T_{GR}. Solar wind velocity was the most consistently correlated over all the data categories (*r* ranging from 0.20 to 0.45), with T_{IMF} also showing reasonably high correlations in some categories ($r = 0.15$–0.50). *Dst* correlations ranged up to $r = 0.35$. T_N and *Bz* were more correlated in some categories than in others (with the highest correlations being 0.45 and 0.38). Plasma density showed much less correlation with T_{GR} (the highest *r* being only 0.22), but it was more correlated with T_{GR} during CME storms than during CIR storms, with *N* showing a negative correlation after the main phase of CIR storms. Both *V* and T_{IMF} show a much stronger correlation with T_{GR} during CME storm initiation than during the initial phase of CIR storms, but the differences between CME and CIR storms are not as marked during the other phases. T_N was also more correlated with T_{GR} in CME than in CIR storms.

4.2. Path Analysis

[34] Using a series of multiple regressions, we constructed path diagrams to show the influence of the independent variables on the magnetospheric ULF activity (Figure 4). The thickness of the arrows in the diagrams corresponds to

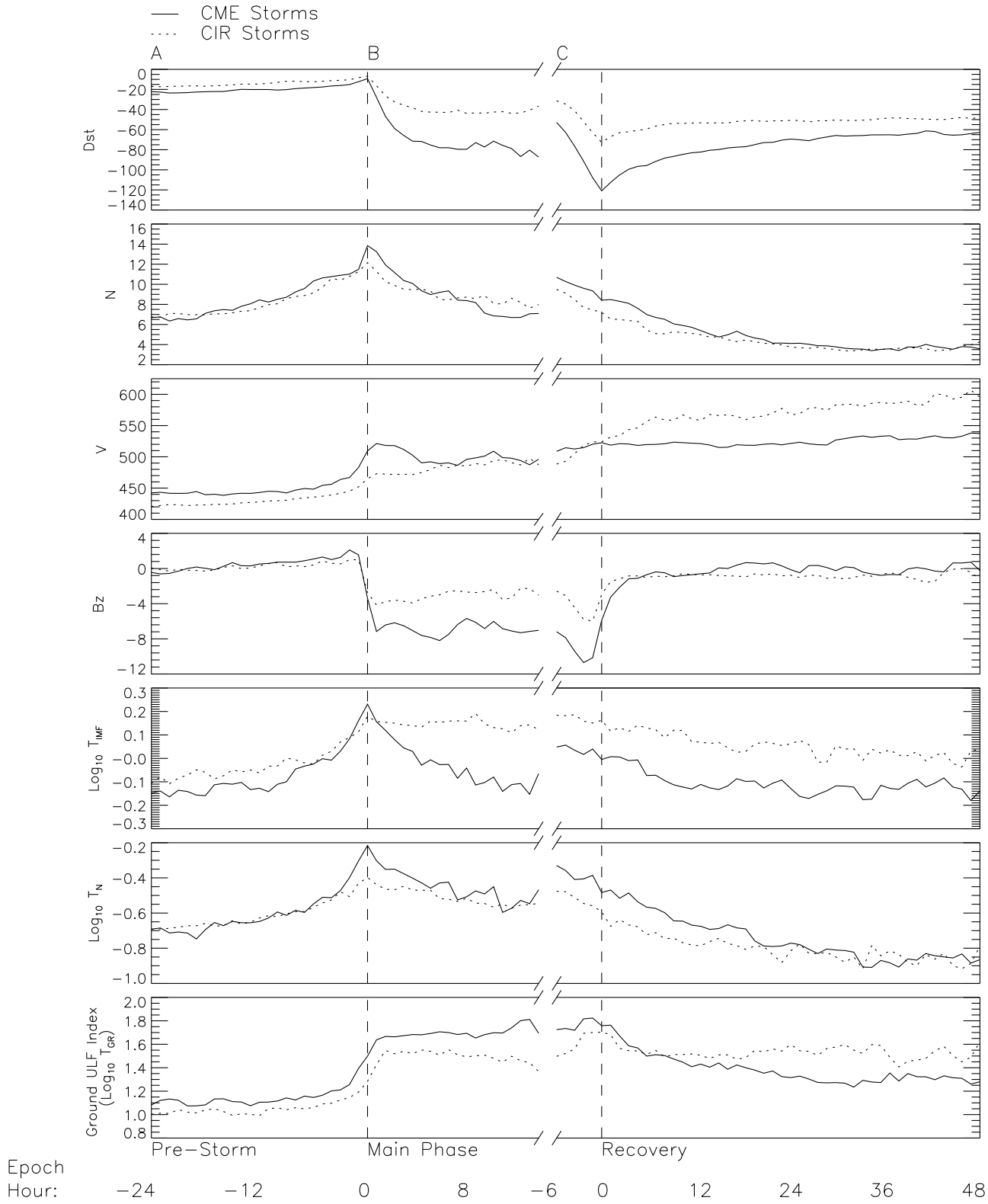

Figure 2. Superposed epoch time plots of the ground ULF index and possible drivers of these ULF waves, averaged over the storms of 1991–2004 that could be classified as CME or CIR. T_{GR}, T_{IMF}, and T_N are log transformed. Using the first drop in *Dst* as the marker between the initial and main phase and the lowest value of *Dst* as the marker between main phase and recovery, hourly data for CME and CIR storms were averaged and plotted as follows: (a) initial (24 h before the start of the main phase); (b) main phase; and (c) 6 h before recovery, the period of recovery, and the time period after recovery.

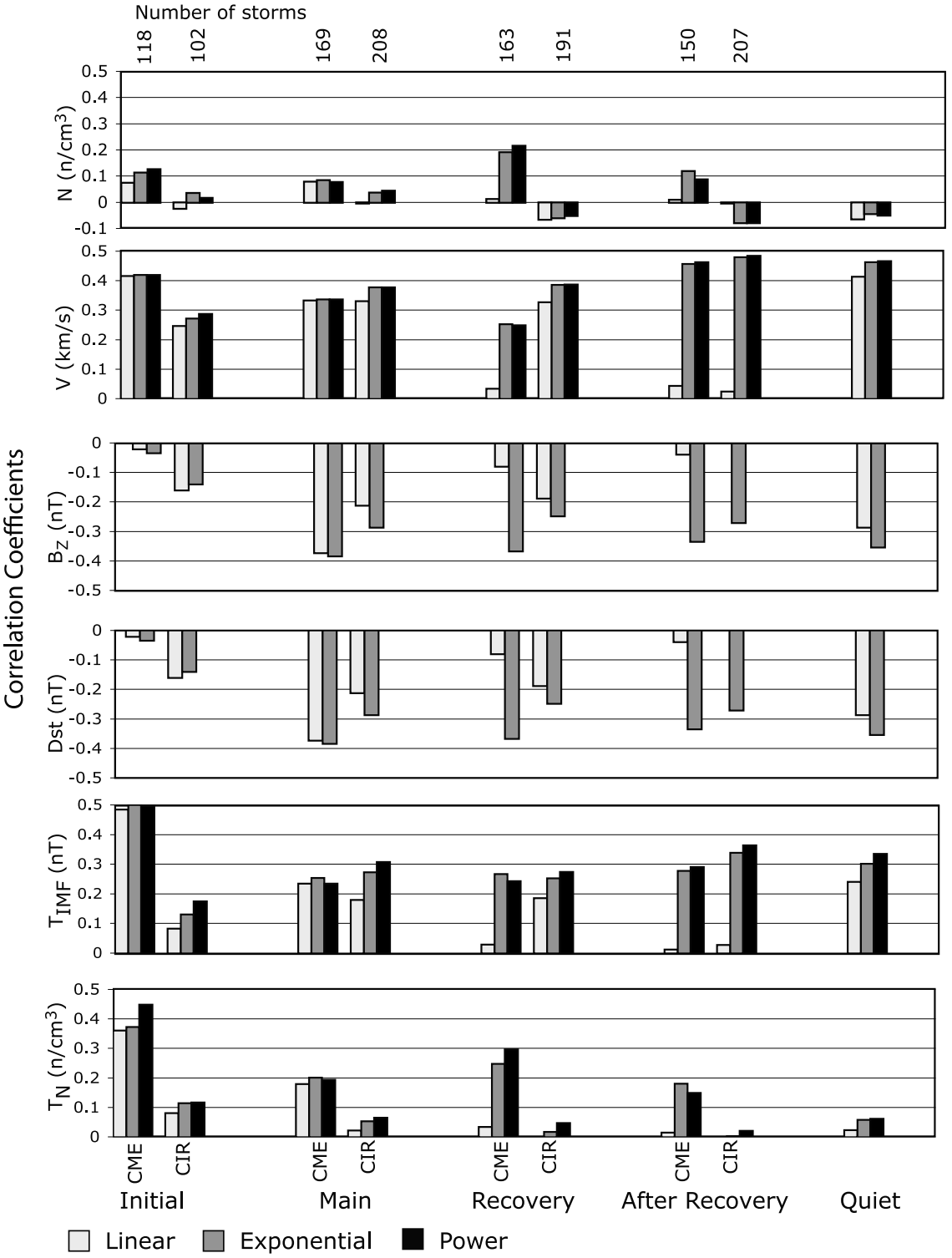

Figure 3. Linear, exponential, and power correlations between T_{GR} and each of T_{IMF}, T_N, N, and V; linear and exponential correlations between T_{GR} and *Dst* and *IMF Bz*.

the standardized partial regression coefficient, showing the influence of that independent variable on the dependent variable. Standardized coefficients were used to allow for easy comparison of the effects of independent parameters within these models. When an independent variable showed a significant effect on T_{GR} (significance being a probability of occurring less than 5% of the time purely by chance, or $P < 0.05$), the arrow from that variable is shown in black. If the effect was not significantly correlated with T_{GR}, that arrow is shown in gray.

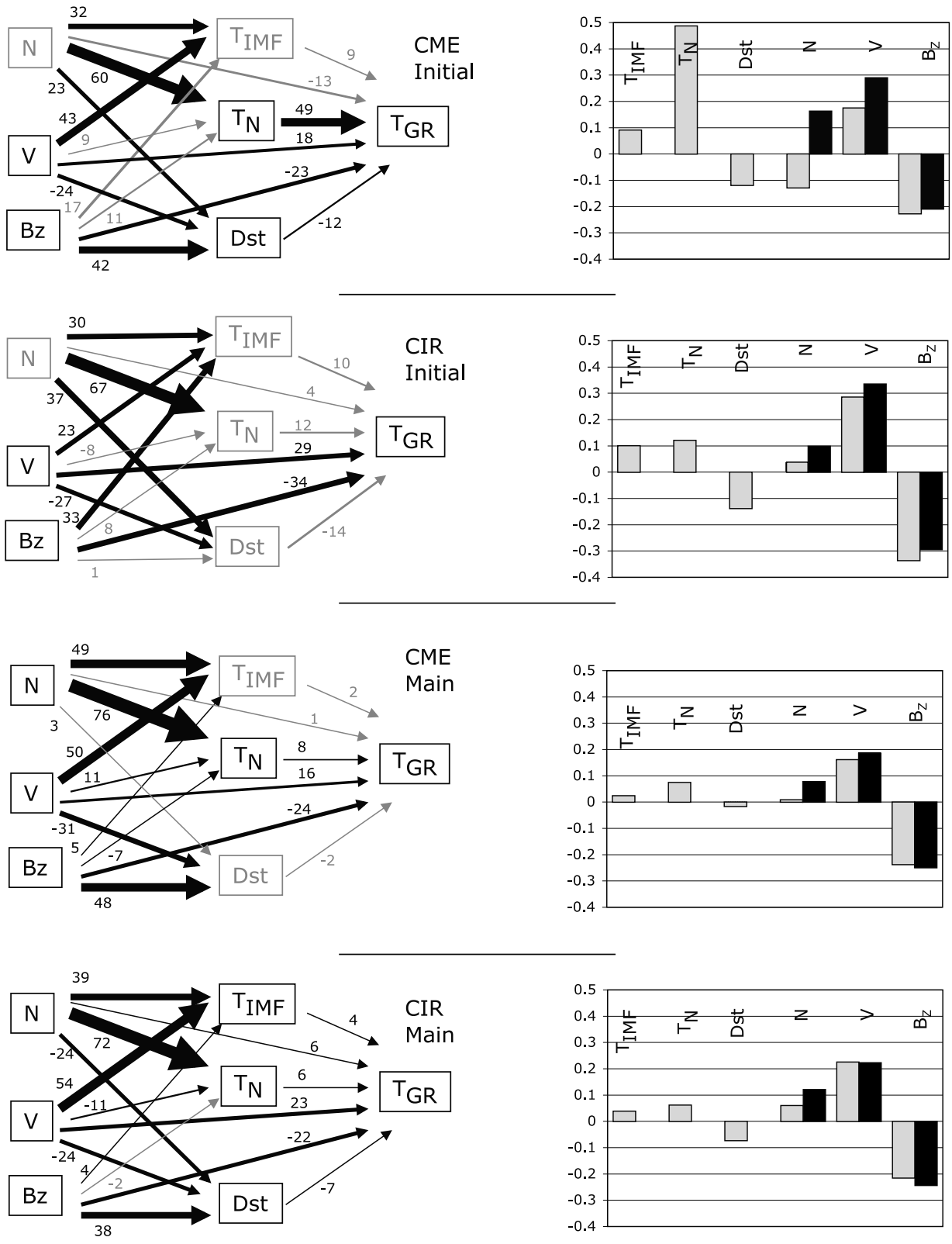

Figure 4. Path diagrams of multiple regression analyses. Numbers associated with each path are the standardized partial regression coefficients × 100. Line thickness of each path corresponds to this partial regression coefficient. Each model includes the lag of T_{GR} (1 h before) as a dependent variable to correct for the problem of serial autocorrelation, but this is not shown in the diagram for reasons of clarity. The bar chart shown with each path diagram compares the magnitude of the direct effects (for all the variables) as well as the sum of the direct and indirect effects of N, *V*, and IMF *Bz*.

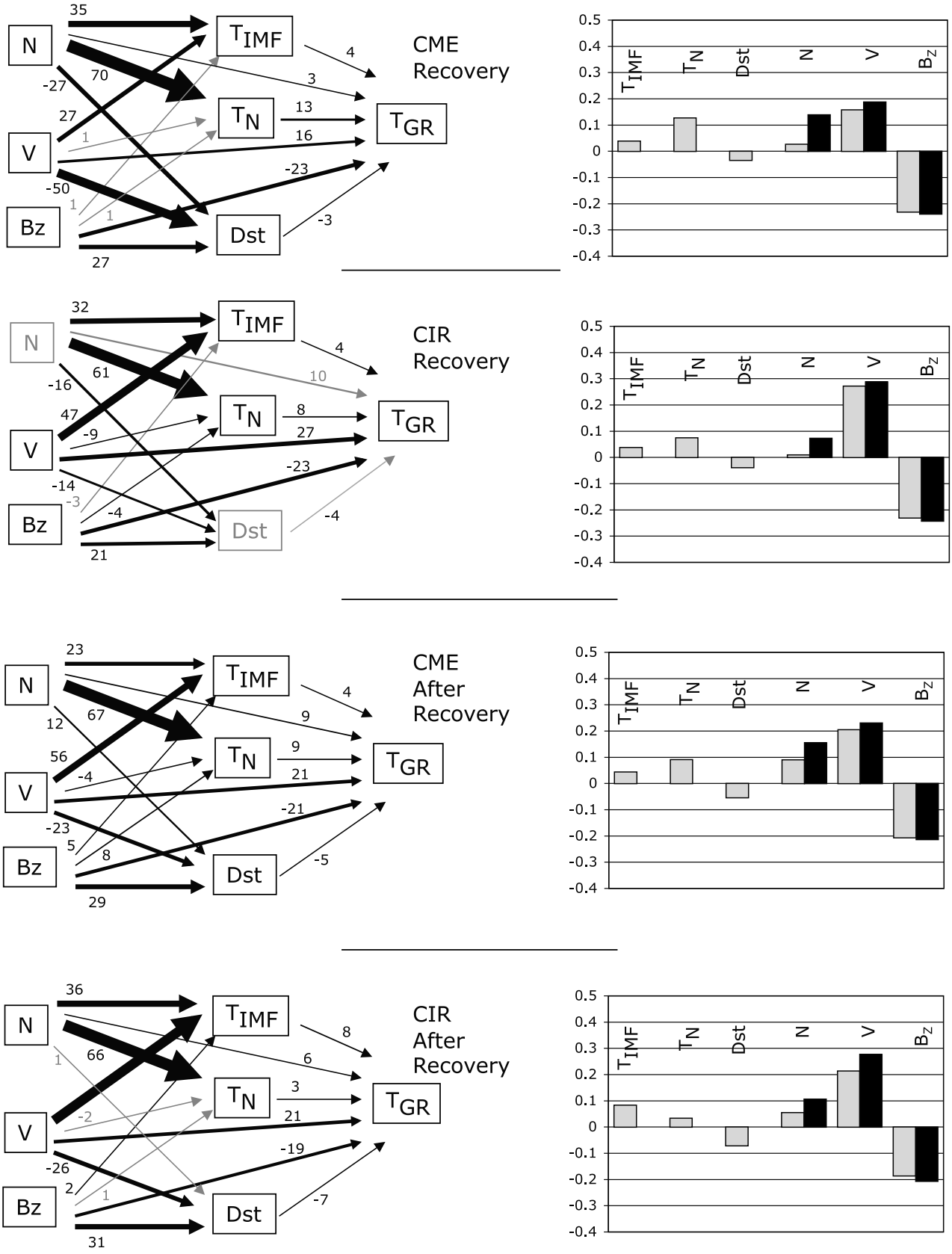

Figure 4. (continued)

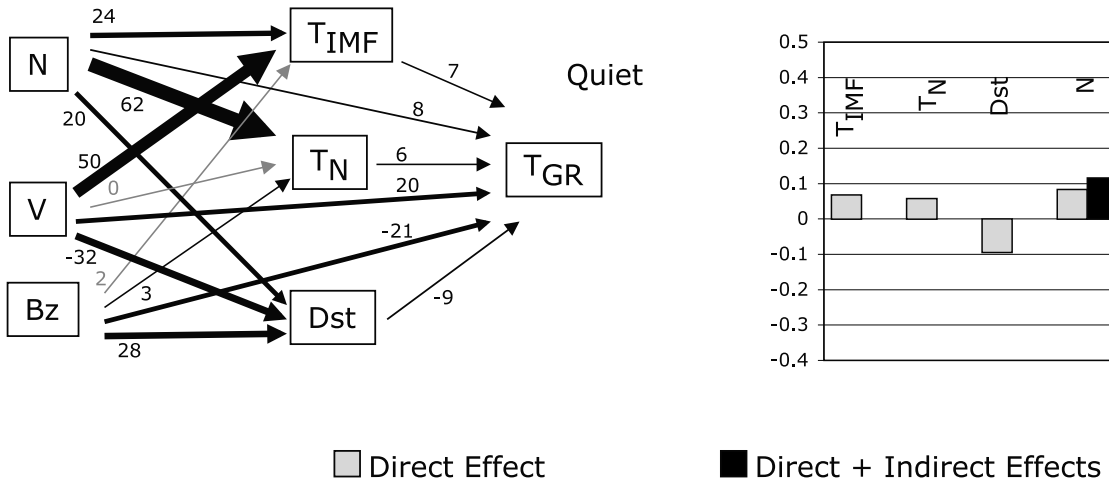

Figure 4. (continued)

[35] The path analyses allow a comparison of the direct influence a predictor variable may have on T_{GR} as well as the influence it may have indirectly through other parameters. The basic solar wind/IMF parameters (N, V, and Bz) are all postulated to influence magnetospheric ULF activity not only on their own but also through the intermediate variables of T_{IMF}, T_N, and Dst that describe the fluctuations of the solar wind/IMF and magnetospheric energetic particle intensity. These indirect effects are represented in the path diagrams by the arrows that originate in N, V, and Bz and go through T_{IMF}, T_N, and Dst to T_{GR}. Indirect effects can be calculated as the sum of the products of the intermediate paths. For example, for the initial storm phase the coefficient of the indirect path from N through T_N to T_{GR} is composed of the coefficient of the path from N to T_N, multiplied by the coefficient of path from T_N to T_{GR}, namely $0.673 \times 0.121 = 0.081$. Bar charts given along with the path diagrams compare the magnitude of the direct effects (for all the variables) as well as the sum of the direct and indirect effects of N, V, and Bz.

[36] When other variables were controlled for in the multiple regressions, V and Bz showed a strong direct influence in all data categories, in keeping with the results of the simple correlations (Figure 3), as well as indirect effects via T_N, T_{IMF}, and Dst. The strong correlations of T_{GR} with T_{IMF}, T_N, and Dst are not as marked in the multiple regressions. Some of these associations are lowered when other variables are also introduced into the analysis. However, although the correlations of T_{GR} with T_{IMF}, T_N, and Dst are lower in the multiple regression, this does not mean T_{IMF}, T_N, and Dst are without influence, only that their influence is less than that of V or IMF Bz.

[37] It is interesting to note, as well, that while T_{IMF} shows a stronger association with T_{GR} than T_N does in the simple correlations, the multiple regressions show the opposite in many data categories. In particular, T_N shows a strong influence during the initial phase of CME storms, greater than any of the other parameters. T_N often has twice the effect of T_{IMF} in the multiple regressions, although in the simple correlations, it was T_{IMF} that showed the strongest association with T_{GR}.

[38] For N and V, the sum of direct and indirect paths shows there is usually a somewhat greater positive correlation with T_{GR} than the direct path alone shows. This is generally more visible with N, because of the strong correlation of N with T_N and thus the strong indirect path through that variable. The sum of direct and indirect paths from IMF Bz also shows a greater correlation than the direct path alone, except during the initial phase when the indirect paths work in the opposite direction from the direct path.

4.3. Prediction of Pc5 Power in the Magnetosphere With the Regression Model

[39] As a predictive model of magnetospheric ULF power, the unstandardized coefficients from the main regression models where T_{GR} is the dependent variable can be used (Table 4). To bring the scale of all variables within an order of magnitude, V was divided by 100, whereas Dst, N, and Bz were divided by 10. This allows for a more compact presentation but does not affect the outcome of the analysis. Table 4 also lists the coefficient of determination R^2 (the fraction of variation in the T_{GR} that can be explained by the model). The square root of R^2 (r) is comparable to the r obtained in simple correlations. Because these are unstandardized coefficients, an intercept term b_0 is also necessary. Future values of T_{GR} can be predicted by multiplying each parameter by the value of the independent variable and summing, as follows:

$$\log_{10}T_{GR} = b_0 + b_1\log_{10}T_N + b_2\log_{10}T_{IMF} + b_3 Dst + b_4 N + b_5 V + b_6 Bz + b_7 Lag T_{GR}. \quad (4)$$

[40] Using the regression model (4), magnetospheric ULF activity at the recovery and postrecovery phases, which are most significant for the prediction of the relativistic electron behavior, can be predicted (nowcasted) from the current solar wind, IMF and Dst values, and from the value of T_{GR} in the previous hour. The correlation in these time periods is

Table 4. Unstandardized Coefficients of the Multiple Regression Analyses[a]

Storm Type	Storm Phase	b_0	$\log_{10} T_{IMF}$	$\log_{10} T_N$	*Dst*/10	*N*/10	*V*/100	*Bz*/10	Lag $\log_{10} T_{GR}$	R^2	*r*
CME	Initial	0.719	0.118	0.550	−0.022	−0.052	0.069	−0.181	0.421	0.647	0.804
CME	Main	0.545	0.024	0.073	−0.001	0.004	0.046	−0.116	0.504	0.535	0.732
CME	Recovery	0.271	0.056	0.144	−0.004	0.027	0.067	−0.194	0.586	0.637	0.798
CME	After recovery	−0.029	0.067	0.117	−0.020	0.077	0.114	−0.239	0.561	0.644	0.803
CIR	Initial	0.264	0.114	0.114	−0.028	0.013	0.112	−0.256	0.431	0.431	0.657
CIR	Main	0.168	0.062	0.073	−0.001	0.035	0.080	−0.194	0.566	0.624	0.790
CIR	Recovery	0.202	0.053	0.099	−0.009	0.010	0.094	−0.312	0.507	0.510	0.714
CIR	After recovery	0.085	0.129	0.050	−0.026	0.076	0.084	−0.315	0.535	0.588	0.767
Quiet		0.008	0.104	0.083	−0.033	0.075	0.104	−0.365	0.538	0.637	0.798
All		0.067	0.098	0.079	−0.010	0.043	0.091	−0.271	0.574	0.674	0.821

[a]$\text{Log}_{10} T_{GR}$ is the dependent variable.

somewhat better for CME storms, ≈0.80, than for CIR storms, ≈0.71–0.77. When all data are combined (all storm categories and quiet), the correlation coefficient is 0.82.

4.4. Statistical Differences Between CME and CIR Storms

[41] This analysis is designed to determine whether the magnetospheric ULF wave activity varies between CME and CIR storms, as well as being influenced by the other independent variables. The partial standardized regression coefficients determined from the regression analyses in which storm type is used as an independent variable are shown in Figure 5. T_{GR} varies by storm type during the main phase, recovery, and the 48 h after recovery. It is larger during CME storms during the main phase and recovery but larger during CIR storms in the period after recovery. However, there is no statistical difference in the T_{GR} between CME and CIR storms during the initial phase. As in the previous analyses of the solar wind and IMF parameters, *V* and IMF *Bz* show the most influence on T_{GR}, although the other parameters are, in general, still statistically significant.

[42] The effects of *N* vary little between storm types, but the other variables show differences. *Dst* has a greater effect in CME storms only during the main phase, whereas *Bz* shows a moderately stronger effect during the main phase, recovery, and after recovery in CME storms. The effect of *V* varies, depending on the storm phase, with its effect being stronger during CIR storms in the main phase and recovery but stronger during CME storms in the period after recovery. These changing influences can also be seen in the bar charts of Figure 4.

[43] Figure 5 also gives the standardized partial regression coefficients for the statistical interactions between storm type and the other independent variables. These interaction terms describe the difference in the effect of a given parameter at different levels of a second parameter, with a positive coefficient indicating a greater effect in CME storms.

[44] The significant "storm type × T_N" interaction shows that T_N has a greater effect in CME storms during initial phase, recovery, and the 48 h after recovery, but an equal effect between storm types during the main phase of the storm. The greatest difference in the effect of T_N between storm types occurs during the initial phase. This difference is also visible in Figure 4 CME and CIR initial phase, where the T_N coefficient is much greater in CME storms than CIR storms. This differing effect of T_N is not as obvious in recovery and after recovery (Figure 4), but it is still present. Thus, the "precursory" increase of T_N is most noticeable for CME storms.

5. Discussion

[45] Previous studies, referenced in section 1, have shown a strong association of Pc5 waves with solar wind velocity. In the present study we confirm that velocity has a positive direct influence on Pc5 wave power but that this effect can be enhanced by its influence on other parameters associated with Pc5 waves such as T_N, T_{IMF}, and *Dst*. In addition, although plasma density (*N*) often shows little influence on its own because of its indirect influence on Pc5 wave power through T_N, the overall effect of *N* was often appreciable.

[46] A similar situation exists between IMF *Bz* and *Dst*. In the simple correlations, *Dst* appears to have a strong influence on T_{GR}; however, this effect is lower in the multiple regression. In this case, it appears to be the correlation of *IMF Bz* with *Dst* that is causing more apparent correlation between *Dst* and T_{GR}. The addition of *Dst* as a representation of the ring current intensity to the model is perhaps not as critical as some other variables.

[47] In addition to the previously studied associations of basic solar wind and IMF parameters with the magnetospheric ULF wave power, we have also shown associations of T_{GR} with the fluctuations of both the plasma density (T_N) and of the IMF (T_{IMF}). This was most prominent during storm recovery and the 48 h period after recovery.

[48] Previous studies have shown a power law dependence between velocity and Pc5 power [*Engebretson et al.*, 1998; *Pahud et al.*, 2009], but our data show that the lack of fit with a linear model extends to other predictive parameters as well.

[49] Time plots of the variables show that more than one factor is responsible for driving the Pc5 waves. *V* and IMF *Bz* track the T_{GR} plot more closely, but even these two independent variables do not correlate with the T_{GR} exactly. *N* and T_N, as well as T_{IMF} in CME storms, peak early, at onset, correlating with the initial rise in T_{GR}, but they fall off as the storms progress through the main phase and recovery, while Pc5 wave activity continues to climb even after its initial surge. Thus, while it may be that these independent variables are predictive of the initial growth of the Pc5 wave power, they cannot be responsible for the continued rise during the main phase and the maintenance of these waves into recovery. The lack of a better correspondence between

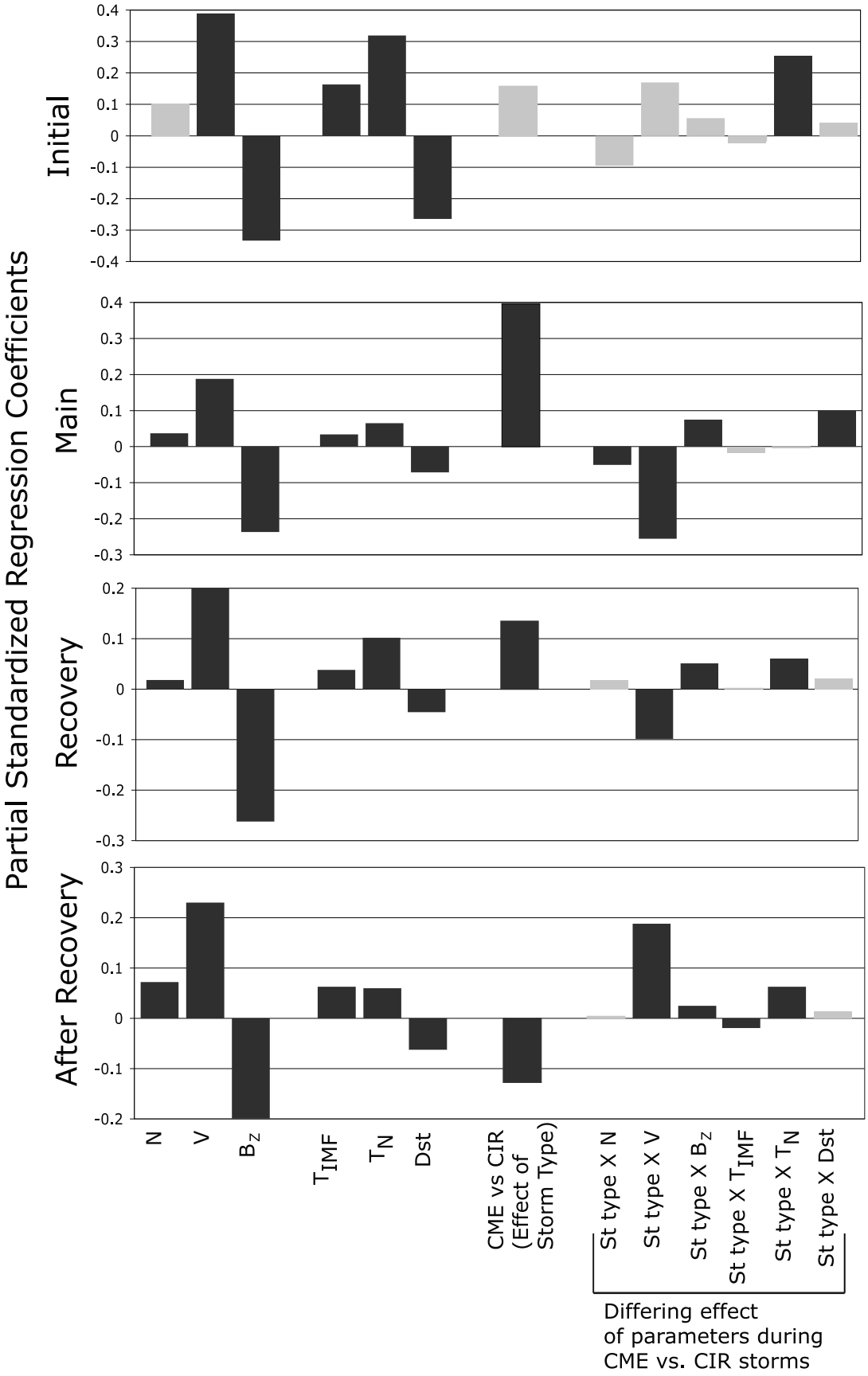
Partial Standardized Regression Coefficients
Initial
Main
Recovery
After Recovery
N
V
B_z
T_{IMF}
T_N
Dst
CME vs CIR (Effect of Storm Type)
St type X N
St type X V
St type X B_z
St type X T_{IMF}
St type X T_N
St type X Dst
Differing effect of parameters during CME vs. CIR storms

Figure 5

T_{GR} and any one of these independent variables suggests that the T_{GR} may be responding to all these variables simultaneously. One of the implications of this result is that a sufficiently high solar wind flow velocity, widely supposed to be the key factor for the Kelvin-Helmoltz instability, is a necessary but not sufficient condition. Probably, additional triggering is necessary. This argues for the multifactor analyses that we present in the multiple regression and path analyses.

[50] We have chosen in this study to use the measured parameters from the solar wind and IMF (N, V, and Bz) rather than the derived parameters that are often used (P and Ey). The predictive value of the models is greater with the three measured parameters included in a multiple regression than with the two derived parameters (Table 3). Given this, it seems preferable to use measured parameters rather than derived variables in modeling Pc5 activity. The attractiveness of the derived variables lies in their ability to bring together two of the measured variables in predicting Pc5 activity in one parameter (N and V in the case of P, and V and Bz in the case of Ey), but this same goal can be accomplished more completely and with more detail by simply using all three of N, V, and Bz in a multiple regression model.

[51] Although the simple paired correlations (Figure 3) suggest most of the possible factors might influence the ground ULF wave power index, the relative importance of factors changes when they are analyzed together in a multiple regression (Figure 4). One striking example is the high simple correlation of the IMF variability T_{IMF} with T_{GR}. This dependence drops to a much lower level when all the explanatory variables are added to the model. T_{IMF} is itself strongly influenced by V, as can be seen in the path diagrams. Although both V and T_{IMF} show a strong correlation with T_{GR} in the simple correlations, when both are entered in the multiple regression model, this influence is shared between them, with the bulk of it coming from the solar wind velocity. This is not to say that T_{IMF} has no influence on its own. The multiple regression shows that despite the high correlation of T_{IMF} with V, T_{IMF} has its own effect on T_{GR} independent of V. Without the knowledge gained from the multiple regression, there would be no way to determine whether T_{IMF} was correlated with T_{GR} in its own right or whether the apparent correlation was only because both T_{IMF} and T_{GR} were each influenced by V without any relation between T_{IMF} and T_{GR}. The multiple regression tells us that T_{IMF} does have an identifiable direct effect on T_{GR} on its own but that a portion of the correlation seen between T_{IMF} and T_{GR} in the simple correlations is of a spurious nature.

[52] The path from N to T_{IMF} is also considerable, although not as great as that from V. Although N is not as associated with T_{GR} as V, its correlation with T_{IMF} also lowers the direct T_{IMF} effect on T_{GR} in the multiple regression. N also has a large influence on T_N, which is not surprising as the fluctuations in N can be expected to increase as N increases, there being more room for variation with a larger value. This correlation results in the indirect effects of N (through both T_N and T_{IMF}) being as large or larger than N's direct influence. Thus, while plasma density showed little influence on its own, because of its indirect influence on T_{GR} through T_{IMF} and T_N, the overall effect of N was often appreciable. This conflicts with the conclusion that might be made from the simple correlations alone, where N would have been seen as an insignificant factor.

[53] However, despite the fact that some of the simple correlation between T_{IMF} and T_N with T_{GR} can be explained by both T_{IMF} and T_N being also correlated with V and N, there is a remaining fraction of correlation that both T_{IMF} and T_N have with T_{GR}. This confirms statistically the findings of events when Pc5 fluctuations in the Earth's magnetosphere can be attributed to fluctuations in the solar wind and IMF of the same frequency [*Kepko et al.*, 2002; *Takahashi and Ukhorskiy*, 2007, 2008; *Villante et al.*, 2007; *Kessel*, 2008]. However, our study provides stronger support for this hypothesis in that we have separated out the contributions of V, N, Bz, and Dst so that the contributions of fluctuations in N and IMF can be assessed independently.

[54] In this study, by the use of multiple regression, we have achieved a model that accounts for more of the variation in Pc5 power than that reported in previous studies. The highest correlation obtained by *Takahashi and Ukhorskiy* [2007, 2008] in their analysis of the relationship between pressure and Pc5 wave power was approximately 0.7. When this is squared to obtain the equivalent coefficient of determination R^2, this results in an R^2 value of only 0.49. The comparable multiple regression analysis in our study (combining all data, both storm and quiet) gives a much higher R^2 of 0.67. Moreover, *Takahashi and Ukhorskiy* [2007] studied the year of solar maximum when high solar wind streams are very rare. As a statistical dependence between T_{GR} and V is only seen above a threshold solar wind velocity ~400 km/s [*Romanova et al.*, 2007], it is not surprising that the *Takahashi and Ukhorskiy* [2007] analysis shows the dominating interplanetary factor controlling magnetospheric Pc5 activity to be the power of pressure fluctuations, similar to T_N, instead of V.

[55] In addition to studying the relationship of independent factors with Pc5 wave activity, it may also be possible to nowcast Pc5 activity by inserting current measurements of the independent parameters into the regression equation (4). This equation can be used as a predictive model of Pc5 activity with the b coefficients determined from data inputs (the unstandardized coefficients from Table 4). It may seem an obvious step to attempt to predict a subset of the current data set with these coefficients, but using the regression

Figure 5. Standardized partial regression coefficients for the larger multiple regression model in which storm type (CME versus CIR) and the interactions of the other parameters with storm type are all added as independent variables. Storm type is represented by an indicator variable with CME storms coded as 1, CIR storms as −1. A positive value for the storm type coefficient indicates that CME storms show higher T_{GR} than CIR storms. The interaction terms (storm type × T_N, for example) show the different effect the same level of a variable may have during CME versus CIR storms. A positive interaction coefficient indicates that this parameter has a stronger effect during CME storms; a negative coefficient indicates the effect is stronger during CIR storms. Black bars indicate when the effect is statistically significant ($P < 0.05$).

coefficients from this study to "predict' a subset of the data used to obtain the coefficients is not an appropriate way to validate the model. Validation cannot be done with the same data that was used to produce the model, so this validation would be suitable as a future study. Further work may elucidate the level of accuracy of these predictions. After a proper validation, the regression model can be used to nowcast the expected level of the ULF wave power in the magnetosphere. Development of similar models, using Pc5 power in the magnetosphere as a predictor variable along with solar wind and IMF parameters, could eventually be used to evaluate the diffusion coefficients of the relativistic electrons, parameterized by the solar wind/IMF values.

[56] During the initial and main phase of storms, ground Pc5 variations are greater in CME storms than in CIR storms, but this activity falls off more quickly after recovery in CME storms (Figure 1). Pc5 activity may be stronger in the main phase of CME storms because CME storms are, on average, stronger storms [*Borovsky and Denton*, 2006].

[57] The solar wind parameters differ between CME and CIR storms as well (Figure 1), and some of the differences in ground Pc5 activity may be attributed to the variation in the independent variables. However, this is not the whole story. In this paper, we have demonstrated, through the analysis of interactions in a multiple regression model that the response of the ground Pc5 to solar wind parameters also varies between CME and CIR storms, even when the solar wind velocity and IMF are of similar intensity. For example, V has more influence on T_{GR} in CIR storms during the main phase and recovery, whereas Bz has a greater influence in CME storms. The physical insight into this is hard to interpret within the existing paradigm of Pc5 pulsation generation.

6. Summary

[58] We have studied the association of Pc5 power recorded by ground magnetometers with a variety of solar wind parameters, examining the data with multiple regression analysis. Multiple regression allowed us to investigate the influence of all the independent parameters simultaneously and to determine which factors were most influential and which were only correlated with the influential factors. In addition, we used path analysis to study a presumed structure of influence among the variables. This model assumed that number density, velocity, and IMF Bz acted both on Pc5 activity and on the intermediate variables of *Dst* and the variations in number density and IMF. As the measured variables (velocity, number density, and IMF Bz) explained more of the variation in a multiple regression model than derived parameters that are often used in these studies (pressure and the solar wind electric field), we performed our analyses using the measured variables.

[59] In both storm types (CME and CIR) and during all storm phases (initial phase, main phase, recovery, and a 48 h period after recovery) as well as during quiet periods, solar wind velocity and IMF Bz influenced ground Pc5 activity directly, whereas the number density was of less influence. These two variables also acted on Pc5 indirectly through the intermediate parameters of *Dst*, and the variation in number density and in IMF, although at a weaker level. Fluctuations in both number density and IMF B were of less direct influence than solar wind velocity and the average IMF Bz, but multiple regression analysis showed that the correlation of these fluctuations with the ground Pc5 power is a real phenomenon and not the result of both T_{GR} and the fluctuations of N and IMF B being each separately correlated with the average values of V and IMF Bz. The 1 h lag term of T_{GR} also showed a high correlation with the current value of T_{GR}, demonstrating that Pc5 fluctuations in the previous hour have a strong influence on current values.

[60] Several of the independent variables differed between storm type (CME and CIR). This accounted for some of the difference in Pc5 activity between storm types, but in addition, the effect of certain independent variables differed depending on storm type, their influence differing depending on whether the storm was CME or CIR.

[61] A regression model offers the possibility of predicting Pc5 wave power levels in the magnetosphere using current values of solar wind and IMF variables. As Pc5 wave power, along with solar wind parameters, are also correlated with relativistic electrons in the radiation belt, future models may be developed that will nowcast the expected diffusion coefficients of these electrons from ground based Pc5 data and these solar wind and IMF factors.

[62] This statistical model allows the nowcasting of the level of global ULF wave activity from the interplanetary and geomagnetic parameters for the first time. This new statistical approach can be applied to other problems of solar-terrestrial relationships, where independent contributions from many external factors are to be identified. The results obtained are important for ULF wave physics, because they show statistically the relative contribution of the main ULF drivers to the magnetospheric ULF power.

[63] **Acknowledgments.** This work was supported by NSF grant ATM-0827903. Solar wind and IMF parameters were obtained from the OMNI data site (omniweb.gsfc.nasa.gov) at NSSDC. The ULF wave index is available at the anonymous FTP site space.augsburg.edu, in the folder:/MACCS/ULF-Index/or upon request from the authors. We thank the two reviewers for their helpful comments.

[64] Masaki Fujimoto thanks Richard Denton and another reviewer for their assistance in evaluating this paper.

References

Alves, M. V., E. Echer, and W. D. Gonzalez (2006), Geoeffectiveness of corotating interaction regions as measured by *Dst* index, *J. Geophys. Res.*, *111*, A07S05, doi:10.1029/2005JA011379.

Baker, G. J., E. F. Donovan, and B. J. Jackel (2003), A comprehensive survey of auroral latitude Pc5 pulsation characteristics, *J. Geophys. Res.*, *108*(A10), 1384, doi:10.1029/2002JA009801.

Borovsky, J. E., and M. H. Denton (2006), Differences between CME-driven storms and CIR-driven storms, *J. Geophys. Res.*, *111*, A07S08, doi:10.1029/2005JA011447.

Borovsky, J. E., and H. O. Funsten (2003), Role of solar wind turbulence in the coupling of the solar wind to the Earth's magnetosphere, *J. Geophys. Res.*, *108*(A6), 1246, doi:10.1029/2002JA009601.

Denton, M. H., J. E. Borovsky, R. M. Skoug, M. F. Thomsen, B. Lavraud, M. G. Henderson, R. L. McPherron, J. C. Zhang, and M. W. Liemohn (2006), Geomagnetic storms driven by ICME- and CIR-dominated solar wind, *J. Geophys. Res.*, *111*, A07S07, doi:10.1029/2005JA011436.

Elkington, S. R., M. K. Hudson, and A. A. Chan (2003), Resonant acceleration and diffusion of outer zone electrons in an asymmetric geomagnetic field, *J. Geophys. Res.*, *108*(A3), 1116, doi:10.1029/2001JA009202.

Engebretson, M., K.-H. Glassmeier, M. Stellmacher, W. J. Hughes, and H. Lühr (1998), The dependence of high-latitude Pc5 wave power on solar wind velocity and on the phase of high-speed solar wind streams, *J. Geophys. Res.*, *103*, 26,271–26,384, doi:10.1029/97JA03143.

Eriksson, P. T. I., A. D. M. Walker, and J. A. E. Stephenson (2006), A statistical correlation of Pc5 pulsations and solar wind pressure oscillations, *Adv. Space Res.*, *38*, 1763–1771, doi:10.1016/j.asr.2005.08.023.

Gonzalez, W. D., B. T. Tsurutani, and A. L. Clúa de Gonzalez (1999), Interplanetary origin of geomagnetic storms, *Space Sci. Rev.*, *88*, 529–562.

Greenstadt, E. W., J. V. Olson, P. D. Loewen, H. J. Singer, and C. T. Russell (1979), Correlation of Pc 3, 4, and 5 activity with solar wind speed, *J. Geophys. Res.*, *84*, 6694–6696, doi:10.1029/JA084iA11p06694.

Kepko, L., and H. E. Spence (2003), Observations of discrete, global magnetospheric oscillations directly driven by solar wind density variations, *J. Geophys. Res.*, *108*(A6), 1257, doi:10.1029/2002JA009676.

Kepko, L., H. E. Spence, and H. J. Singer (2002), ULF waves in the solar wind as direct drivers of magnetospheric pulsations, *Geophys. Res. Lett.*, *29*(8), 1197, doi:10.1029/2001GL014405.

Kessel, R. L. (2008), Solar wind excitation of Pc5 fluctuations in the magnetosphere and on the ground, *J. Geophys. Res.*, *113*, A04202, doi:10.1029/2007JA012255.

Kessel, R. L., I. R. Mann, S. F. Fung, D. K. Milling, and N. O'Connell (2004), Correlation of Pc5 wave power inside and outside the magnetosphere during high-speed streams, *Ann. Geophys.*, *22*, 629–641.

Kozyreva, O. V., V. A. Pilipenko, M. J. Engebretson, and K. Yumoto (2007), A new ULF wave index and its comparison with dynamics of geostationary relativistic electrons, *Planet. Space Sci.*, *55*, 755–769.

Loehlin, J. (1991), *Latent Variable Models: An Introduction to Factor, Path and Structural analysis*, Lawrence Erlbaum, Hillsdale, NJ.

Mann, I. R., T. P. O'Brien, and D. K. Milling (2004), Correlations between ULF wave power, solar wind speed, and relativistic electron flux in the magnetosphere: Solar cycle dependence, *J. Atmos. Sol. Terr. Phys.*, *66*, 187–198.

Mathie, R. A., and I. R. Mann (2000), A correlation between the extended intervals of ULF power and storm-time geosynchronous relativistic electron flux enhancements, *Geophys. Res. Lett.*, *27*, 3261–3264, doi:10.1029/2000GL003822.

Mathie, R. A., and I. R. Mann (2001), On the solar wind control of Pc5 ULF pulsation power at mid-latitudes: Implications for MeV electron acceleration in the outer radiation belt, *J. Geophys. Res.*, *106*, 29,783–29,796, doi:10.1029/2001JA000002.

Neter, J., W. Wasserman, and M. H. Kutner (1985), *Applied Linear Statistical Models*, Richard D. Irwin, Inc., Homewood, Ill.

O'Brien, T. P., R. L. McPherron, D. Sornette, G. D. Reeves, R. Friedel, and H. J. Singer (2001), Which magnetic storms produce relativistic electrons at geosynchronous orbit?, *J. Geophys. Res.*, *106*, 15,533–15,544, doi:10.1029/2001JA000052.

Pahud, D. M., I. J. Rae, I. R. Mann, K. R. Murphy, and V. Amalraj (2009), Ground-based Pc5 ULF wave power: Solar wind speed and MLT dependence, *J. Atmos. Sol. Terr. Phys.*, *71*, 1082–1092.

Pilipenko, V., N. Romanova, and L. Simms (2008), ULF wave power index for space weather applications, COST-724 Final Report "Developing the scientific basis for monitoring, modeling and predicting space weather," 279–288, ESA.

Posch, J. L., M. J. Engebretson, V. A. Pilipenko, W. J. Hughes, C. T. Russell, and L. J. Lanzerotti (2003), Characterizing the long-period ULF response to magnetic storms, *J. Geophys. Res.*, *108*(A1), 1029, doi:10.1029/2002JA009386.

Romanova, N., and V. Pilipenko (2009), ULF wave indices to characterize the solar wind-magnetosphere interaction and relativisitic electron dynamics, *Acta Geophys.*, *57*, 158–170, doi:10.2478/s11600-008-0064-4.

Romanova, N., V. Pilipenko, N. Crosby, and O. Khabarova (2007), ULF wave index and its possible applications in space physics, *Bulgarian J. Phys.*, *34*, 136–148.

Takahashi, K., and A. Y. Ukhorskiy (2007), Solar wind control of Pc5 pulsation power at geosynchronous orbit, *J. Geophys. Res.*, *112*, A11205, doi:10.1029/2007JA012483.

Takahashi, K., and A. Y. Ukhorskiy (2008), Timing analysis of the relationship between solar wind parameters and geosynchronous Pc5 amplitude, *J. Geophys. Res.*, *113*, A12204, doi:10.1029/2008JA013327.

Tsurutani, B. T., W. D. Gonzalez, A. L. C. Gonzalez, F. Tang, J. K. Arballo, and M. Okada (1995), Interplanetary origin of geomagnetic activity in the declining phase of the solar cycle, *J. Geophys. Res.*, *100*, 21,717–21,733, doi:10.1029/95JA01476.

Turner, N. E., W. D. Cramer, S. K. Earles, and B. A. Emery (2009), Geoefficiency and energy partitioning in CIR-driven and CME-driven storms, *J. Atmos. Sol. Terr. Phys.*, *71*, 1023–1031.

Vennerstrom, S. (1999), Dayside magnetic ULF power at high latitudes: a possible long-term proxy for the solar wind velocity?, *J. Geophys. Res.*, *104*, 10,145–10,157, doi:10.1029/1999JA900015.

Villante, U., P. Francia, S. Lepidi, et al. (2006) ULF fluctuations of the geomagnetic field and ionospheric sounding measurements at low latitudes during the first CAWSES campaign, *Ann. Geophysicae*, *24*, 1455–1468.

Villante, U., P. Francia, M. Vellante, P. Di Giuseppe, A. Nubile, and M. Piersanti (2007), Long-period oscillations at discrete frequencies: A comparative analysis of ground, magnetospheric, and interplanetary observations, *J. Geophys. Res.*, *112*, A04210, doi:10.1029/2006JA011896.

Yermolaev, Yu. I., N. S. Nikolaeva, I. G. Lodkina, and M. Yu. Yermolaev (2009), Catalog of large-scale solar wind phenomena for the period 1976–2000, *Cosmic Res.*, *47*, 81–94. (original Russian text in *Kosmicheskie Issledovaniya*., *47*, 99–113).

M. J. Engebretson and L. E. Simms, Department of Physics, Augsburg College, 2211 Riverside Ave., Minneapolis, MN 55454, USA. (engebret@augsburg.edu; simmsl@augsburg.edu)

V. A. Pilipenko, Institute of the Physics of the Earth, B. Gruzinskaya 10, Moscow 123995, Russia. (pilipenk@augsburg.edu)